

Polarization-Independent Silicon Metadevices for Efficient Optical Wavefront Control: Supporting Information

Katie E. Chong,[†] Isabelle Staude,^{*,†} Anthony James,[‡] Jason Dominguez,[‡]
Sheng Liu,[‡] Salvatore Campione,[‡] Ganapathi S. Subramania,[‡] Ting S. Luk,[‡]
Manuel Decker,[†] Dragomir N. Neshev,[†] Igal Brener,[‡] and
Yuri S. Kivshar[†]

Nonlinear Physics Centre, Research School of Physics and Engineering, The Australian National University, Canberra ACT 0200, Australia, and Center for Integrated Nanotechnologies, Sandia National Laboratories, Albuquerque, New Mexico 87185, USA

E-mail: isabelle.staude@uni-jena.de

Number of pages: 7

Number of figures: 2

*To whom correspondence should be addressed

[†]Nonlinear Physics Centre, Research School of Physics and Engineering, The Australian National University, Canberra ACT 0200, Australia

[‡]Center for Integrated Nanotechnologies, Sandia National Laboratories, Albuquerque, New Mexico 87185, USA

Sample fabrication

For fabrication of the silicon nanodisk metadevices we performed electron-beam lithography (EBL) on a backside polished silicon-on-insulator wafer (SOITEC, 243 nm top silicon thickness, 3 μm buried oxide thickness) using the negative-tone resist NEB-31A. After cleaning the top silicon surface by oxygen plasma (2 min, 200 W), we first spin-coated HMDS as an adhesion promoter (3000 rpm, 30 s), directly followed by spin-coating the electron-beam resist (3000 rpm, 30 s), resulting in a resist thickness of 300 nm. We performed both a pre-exposure bake (100°C, 2 min) and a post-exposure bake (90°C, 1 min). After electron-beam exposure (400 pA beam), development was performed by inserting the sample into MF-321 developer for 75 s, followed by rinsing it in de-ionized water for several minutes. The resulting resist pattern was then used as an etch mask for an inductively coupled plasma (ICP) etching process (25 W RF power, 300 W ICP power, 60°C) using Ar (40 sccm) and HBr (15 sccm) as etch gases. Ar/Cl₂ plasma chemistry is used for native oxide breakthrough. *Via* in-situ optical monitoring we stopped the etching process when reaching the buried oxide layer. Remaining resist was removed by subsequently inserting the etched sample into an oxygen plasma and piranha solution. Finally, the sample is coated with a 580 nm thick silica layer by low pressure vapor deposition (LPCVD).

Interferometry setup

Figure S1 shows the schematic of the interferometry setup used to optically characterize the wavefront shaping capabilities of the fabricated silicon Huygens' metadvice. A near-infrared tunable laser source is used at the experimental operation wavelength of $\lambda = 1490\text{ nm}$ as a light source. The polarization direction of the output is adjusted by the use of a polarizer (P). The beam is then splitted in two parts using a 50:50 beam-splitter (BS). One part of the laser beam passes the sample (object beam), the other beam path remains empty (reference beam). The two beams are then recombined by a second 50:50 beam-splitter. A piezo stage (PEZ) controls the position of mirror M2 and thus the optical path length

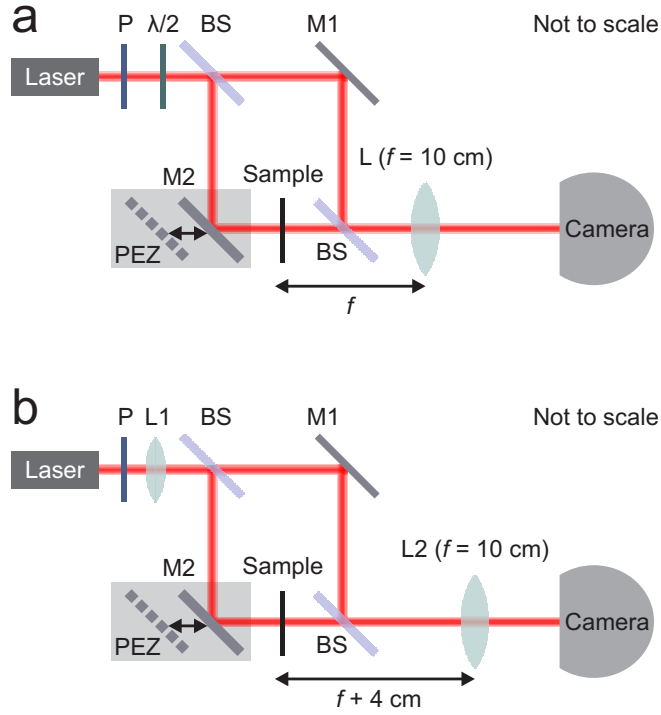


Figure S1: Schematic of the interferometry setup for (a) a direct image of the metasurface and (b) out of focus measurements. P represents the polarizer, BS the polarization-independent 50:50 beam splitters, and M1 and M2 are mirrors. The closed-loop piezo stage (PEZ) is used to control the position of the mirror M2.

of the object beam, while mirror M1 and thus the path length of the reference beam are fixed, thereby allowing for phase reconstruction (for details see corresponding section of the Supporting Information below). A lens of focal length $f = 10$ cm is used to image either the sample plane (Figure S1a) or a plane at 4 cm behind the metasurface (Figure S1b) onto the infrared InGaAs camera, depending on its position in the beam path. In Figure S1a, a $\lambda/2$ -waveplate was inserted to rotate the polarization angle of the incident beam. In Figure S1b, the beam diameter at the sample position was reduced to less than the sample footprint of $500 \mu\text{m} \times 500 \mu\text{m}$ by inserting a weakly focusing lens (L1, $f = 15$ cm) before the first beam splitter.

Polarization independency

In order to provide further experimental evidence of the polarization independency of the beam-shaping functionality of our silicon metadvice, we have performed independent experimental characterization of the vortex beam generated for two perpendicular linear polarizations of the incident laser beam. These results are displayed in Figure S2. As expected, the pronounced zero intensity at the center of the generated vortex beam intensity profile, the characteristic fork structure in the interferogram, and the gradual phase change in the azimuthal direction of the beam with a phase singularity at the center are clearly observed for both polarizations.

Phase reconstruction

To reveal the phase of the propagating light at each quadrant, the four-frame method in phase measurement algorithm¹ is used. The interference fringes in the interferograms are aligned vertically to ease the phase unwrapping process at a later stage. A set of four interferograms $I_j(x, y)$ ($j = 1, 2, 3, 4$) is recorded as the phase shifts between the object and reference beam vary as $(j - 1)\pi/2$ by the control of a closed-loop piezo stage. The prime phase value can then be reconstructed by using the following relation

$$\phi(x, y) = \tan^{-1} \left(\frac{I_4 - I_2}{I_1 - I_3} \right). \quad (1)$$

The phase is unwrapped such that the phase values are no longer bound between $-\pi$ and π and becomes continuous. The average linear background phase gradient in the vertical direction is then extracted from a reference area and subtracted from the unwrapped phase. This process is repeated for the horizontal direction. Finally, to make the phase of the vortex beam clearly visible, the phase is wrapped to 2π again to obtain relative phase values between 0 and 2π .

In Figure 3c, the background phase value is further subtracted from all the phase values

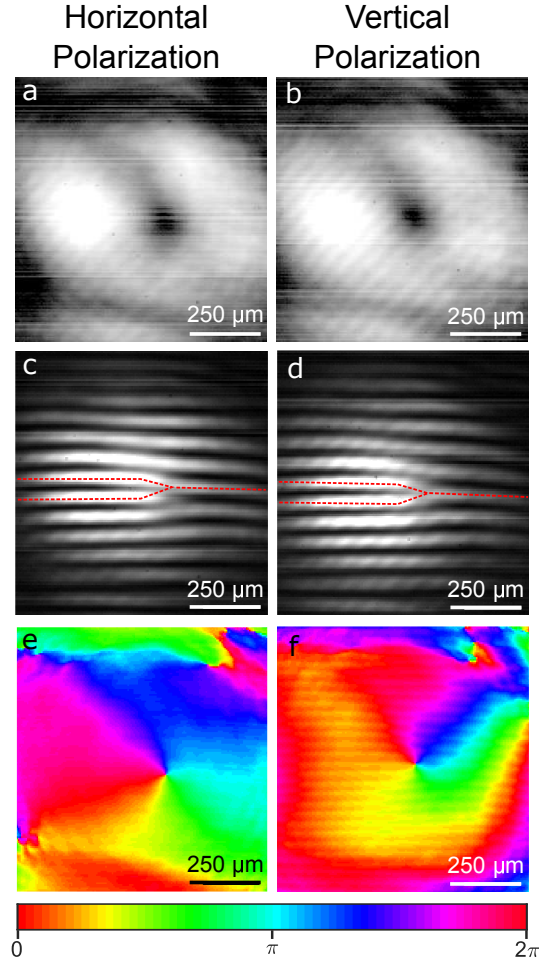


Figure S2: Direct comparison of the beam-shaping functionality of the metadvice for horizontal (left) and vertical (right) polarization. (a,b) Images of the object beam showing the generated vortex beam intensity profile with a minimum at the center. (c,d) Interferograms showing the characteristic fork structure of a vortex beam. (e,f) Reconstructed phases of the object beam imaged at 4 cm beyond the sample (bottom row).

so that they are referenced to the background. The horizontal fringes around the edge of Figure 4c are due to the rewrapping of incompletely eliminated background phase gradient.

Retrieval of the experimental transmittance values

The transmittance is measured separately for each quadrant. Furthermore, we measure the transmittance for an unstructured etched region on the wafer. This allows us to eliminate the effect of the top and bottom interfaces of the layered sample and, together with our knowledge of the transmittance of the silica box layer without the metasurface, to retrieve

the transmitted power T through the combined system of the metasurface and the silica box layer for each quadrant. Note that, as the transmittance of the metasurface alone cannot be separated experimentally by referencing due to the change the metasurface itself causes in the reflectivity of one of the interfaces of the silica box layer.

In our experiment we measure the linear-optical transmittance T_1 through the sample at the position of the metasurfaces forming the quadrants of our metadvice, as well as a reference spectrum through the sample next to the metadvice, T_2 . Commonly, the transmittance of a metasurface referenced to the substrate is determined by simply calculating $\tilde{T} = T_1/T_2$. However, in our present case where the silicon metasurfaces are fabricated from silicon-on-insulator wafers, this simple procedure leads to an overestimation of the metasurface transmittance due to Fabry-Perot oscillations in the silica box layer. This problem arises because the transmittance through the Fabry-Perot cavity formed by the box layer differs significantly for the case with the metasurface, which acts as a frequency-dependent dielectric mirror, as compared to the case of the box layer without the metasurface (T_{box}). Consequently, the transmittance of the metasurface and that of the Fabry-Perot cavity formed by the box layer in the presence of the metasurface cannot be separated by simple referencing to the substrate. However, the combined transmittance of the metasurface and the box layer cavity can be easily retrieved. To this end, we consider the following:

$$\tilde{T} = \frac{T_1}{T_2} = \frac{T T_{UL}}{T_{box} T_{UL}}. \quad (2)$$

Here, T_{UL} denotes the combined transmittance of the upper and lower interfaces of the sandwich structure, which are approximated as identical for the case with and without metasurface. It immediately follows that

$$T = \tilde{T} T_{box}, \quad (3)$$

where \tilde{T} is known experimentally and T_{box} is known analytically as well as numerically with

highest accuracy.

References

- (1) Creath, K. *Progress in Optics*, E. Wolf ed.; Elsevier Science Publishers: Amsterdam, 1988; Vol. XXVI.